19th Brazilian Congress of Thermal Sciences and Engineering
November 06th-10th, 2022, Bento Gonçalves - RS - Brazil

CHARACTERIZATION OF COMBUSTION PARAMETERS IN A SPARK-IGNITION ENGINE USING H_2 AS FUEL

Thompson Diórdinis Metzka Lanzanova
Universidade Federal de Santa Maria
thompson.lanzanova@ufsm.br

Juliano Pereira Silveira
Universidade Federal de Santa Maria
juliano.p.silveira@gmail.com

Andrey Avila da Silva Pereira
Universidade Federal de Santa Maria
andrey.pereira@acad.ufsm.br

Jean Lucca Souza Fagundez
Universidade Federal de Santa Maria
jean.fagundez@acad.ufsm.br

Vinícius Rückert Roso
Universidade Federal de Santa Maria
vinicius.roso@mecanica.ufsm.br

Mario Eduardo Santos Martins
Universidade Federal de Santa Maria
mario@mecanica.ufsm.br

Nina Paula Gonçalves Salau
Universidade Federal de Santa Maria
ninasalau@ufsm.br

Abstract. *In the search for novel fuels that can reduce both greenhouse gas (GHG) and pollutant emissions of the transport sector, hydrogen appears as a promising alternative capable of zeroing vehicle CO_2 emissions, being considered one of the fuels of the future. However, for relevant GHG emissions reduction when using H_2, its production must be clean and renewable, such as from water electrolysis provided no fossil energy is used in the process. In such cases, the hydrogen obtained has zero well-to-wheel CO_2 emissions and it is called green hydrogen. The simple application of hydrogen as a fuel in internal combustion engines is well known and was studied several decades ago. Nevertheless, it was not taken as a serious solution until recently and its use with modern engine technology is still not completely developed. In this regard, this work aims to investigate some operating conditions and combustion characteristics of H_2 in a spark-ignition engine with port fuel injection. Six load conditions were analyzed: 2.3, 3.1, 3.8, 4.4 bar IMEP, with excess air ratio (λ) varying from 2.0 up to 4.3. Combustion and performance variables such as IMEP, COV_{IMEP} and indicated efficiency were evaluated. All tests were conducted aiming at reaching minimum spark advance for best torque (MBT). The results showed that operation was stable even with high λ such as 4.3. In addition, indicated efficiency was up to 36% from excess air ratio from 2.0 to 2.4, considerably higher than when operating the same engine at lower loads with ethanol or Brazilian gasoline under stoichiometric conditions. Thus, the operation with H_2 showed potential for high engine efficiency while decarbonizing vehicle emissions.*

Keywords: *hydrogen, internal combustion engine, combustion, lean operation.*

1. INTRODUCTION

Climate change and strict environmental legislation have accelerated the search for renewable and clean energy sources that can reduce the economic and environmental impact of fossil fuel dependence. In 2016, the Paris Agreement (UNCC, 2016) went into effect to limit CO2 emissions and prevent dangerous climate change by limiting global warming below 2°C and striving to limit it to 1.5°C. However, as reported by the most recent available data of the Intergovernmental Panel on Climate Change (IPCC, 2021), an internationally recognized authority on climate change, without reducing carbon dioxide (CO2) and other greenhouse gases, the goals of the Paris Agreement will not be met. As a result, the report emphasized the imperative of reducing methane emissions by 33% by 2030. Over a 20-year period, methane is 80 times more potent at global warming than carbon dioxide. Energy is responsible for 73.2% of global greenhouse gas emissions, and the transport sector alone emits 16.2% from fossil fuel combustion (Our World in Data, 2020).

Transport is facing a growing challenge, not only from the emissions of greenhouse gases resulting from fossil fuel combustion, but also from market price rises for commodities. Brent crude oil price peaked at $139,00 a barrel in 2022, surpassing a 14-year high (Reuters, 2022), whose economic impact is felt mainly in Brazil due to the depreciation of the Brazilian real. Brazil's current economic situation highlights the need for alternative fuels for sustainable mobility.

Green or renewable hydrogen, i. e. hydrogen produced from renewable sources, is indeed the fuel of the future and plays a key role in a clean future. Highly combustible, hydrogen has the potential to replace fossil fuels as a carbon-free source of energy (IEA, 2019). Brazil is particularly well positioned to be a major hub for green hydrogen development, given the country's abundant natural resources (especially hydro, wind, and solar power plants). Recently, the Brazilian government launched the National Hydrogen Program (PNH2) (MME, 2021), aimed at creating a legal framework for the use of energy from hydrogen and a stable regulatory environment for the green hydrogen market in Brazil to be part of one of the least carbon-intensive energy matrices in the world.

Hydrogen from renewable sources (e.g. solar or wind) can be produced through various pathways such as electrolysis, biohydrogen, thermochemical cycles, photocatalysis, and plasmolysis. Electrolysis meets about 4% of the world's hydrogen demand. Although a promising option for carbon-free hydrogen production, electrolysis faces the challenges of producing hydrogen in a cost-competitive fashion (Younas et. al, 2022; Al-Buraiki and Al-Sharafi, 2022). Currently, the steam reforming process using fossil natural gas is widely used in the chemical industry and accounts for 50% of the hydrogen produced worldwide (César et. al, 2019). Similar to fossil natural gas, biogas can be an alternative renewable source for conventional steam reforming technology to expand green hydrogen production (Minutillo et al., 2020).

The use of hydrogen in internal combustion engines may provide several benefits regarding greenhouse gas and local gaseous pollutants reduction, but it also increases engine control complexity due to several challenges. Hydrogen is a highly reactive fuel when compared to conventional ICE fuels. It presents very low activation energy (0.02 MJ against 0.25, 0.23, and 0.28 MJ of gasoline, ethanol, and methane, respectively) which eases hot-spot autoignition. It has broader flammability limits, and it diffuses on air more than three times faster than methane and more than thirty times faster than ethanol, thus, highly increasing the backfire propensity from the cylinder to the intake system. Additionally, hydrogen presents very high laminar flame speeds, which also tend to increase detonation (knock) propensity for near stoichiometric operation. On the other hand, it has a high autoignition temperature which may provide difficult pure compression ignition control. The stoichiometric air/fuel ratio is much higher than other fuels due to the low H_2 molecular mass, but it presents a much higher lower heating value (LHV) than other fuels (119.70 against 46.72 MJ.kg-1 of H_2 and CH_4, respectively (Heywood, 2018)) which results in high LHV per kilogram of the stoichiometric mixture (3.40 against 2.76, 2.82 and 2.72 MJ.kg-1 of gasoline, ethanol, and methane, respectively). Thus, H_2 is a highly energy-intensive fuel that requires specific engine configurations and control strategies for efficient operation. On top of this, there are the requirements of early intake valve closure (EIVC) instead of late intake valve closure (LIVC) when using over-expanded cycle concepts with port fueling. This is due to the natural in-cylinder mixture backflow while using LIVC which increases intake charge temperature, rising to backfire propensity. Another important requirement is the lower effective compression ratio for successful knock control. H_2 has a much higher knock propensity than conventional fuels due to the high laminar flame speed and low activation energy required for autoignition, in opposition to its high research octane number (RON 130 against 120, 109, and 95 RON of CH_3, ethanol, and Brazilian fuel pump gasohol, respectively).

Several authors already studied H_2 as fuel in spark-ignition engines (Verhelst et al., 2006). A dedicated H_2 four-cylinder 2,4 L spark ignition engine with throttle load control operating at λ 1.0 up to 2.2 (for gross IMEP values varying between 3.56 and 5.60 bar) reached brake thermal efficiencies up to 34.2% (Lee et al., 2019). NO_X emissions for λ higher than 1.8 dropped to less than 30 ppm against more than 4000 ppm at stoichiometric conditions. Another work on a 2.5L engine reported NO_X emissions reduction from more than 4200 ppm to around 1200 ppm at 1200 rpm WOT turbocharged operation when adding up 18% EGR for a λ of 1.67 (Krishnan Unni et al., 2017). A very complete work developed by FORD (Tang et al., 2002) demonstrated stable H_2 engine operation for excess air ratios up to 4.5. It was also reported the possibility to achieve more than 50% indicated thermal efficiencies for λ around 2 at 5000 rpm. Another important piece of information from that work was a large NO_X data library showing that for higher than 2 excess air ratio values, NO_X emissions always dropped below 100 ppm, regardless of engine load and speed.

Due to the high potential of H_2 as an internal combustion fuel, this work presents a preliminary investigation of the combustion characteristics of H_2 in a spark ignition (SI) single-cylinder research engine with port fuel injection. The main objective was to explore the lean dilution limit while using near wide-open throttle (around 95 kPa) operation, in order to understand the control difficulties which would need to be overcome in developing a new highly efficient and low pollutant H_2 engine.

2. METHODOLOGY

A Ricardo Proteus four-stroke single-cylinder research engine was used to evaluate the hydrogen potential as fuel for spark-ignition engines. The engine was modified from compression ignition to spark ignition operation by changing the direct diesel injector system for a centrally mounted spark plug and a commercial CNG port fuel injector. The compression ratio was also modified from 16:1 to 11.7:1 by the use of a metallic spacer between the engine block and the liner block. The diesel bowl-in-piston combustion chamber was not mechanically modified except for the increase in the dead volume caused by the addition of the compression ratio spacer modifier. Table 1 shows the more important test engine specifications.

Table 1. Single-cylinder research engine specifications

Air Supply	Naturally Aspirated
Fuel Supply	Port fuel injection
Stroke	128 mm
Bore	109 mm
Displacement Volume	1194 cm³
Geometric Compression Ratio	11.7:1
Intake Valve Diameter	45 mm
Exhaust Valve Diameter	39 mm
Valves per Cylinder	2

The engine operating parameters (injection pulse width and spark timing) were controlled by a FuelTech FT450 electronic control unit (ECU) in n-alpha (engine speed - throttle position angle) control mode. The crank angle reference for the ECU was derived from a Dynapar B58N 3600 pulses per revolution incremental encoder directly connected to the engine crankshaft. The raw 1440 pulse signal was electronically divided into 60 equally spaced pulses per revolution and the encoder trigger signal was used to reference the top dead center, resulting in a 60-2 signal for the ECU. An open-loop lambda control strategy was used with an exhaust gas oxygen sensor Bosch broadband LSU 4.9 and an ETAS LA4 conditioner unit. This unit presented the capability to read oxygen concentration in the exhaust gases, which was used instead of direct excess air ratio (lambda) measurement. Later, during data post processing, lambda was calculated for each O_2 concentration. This method was used instead of excess air ratio measurement due to the fact that all lambda conditioner units use carbon-based fuels for the stoichiometric air-fuel ratio calculation. Thus, when pure hydrogen is used, a conventional system would provide erroneous excess air ratio values.

Engine-out emissions were measured with an AVL SESAM i60 FT SII, a multi-component automotive exhaust gas analysis system, based on a spectroscopy analyzer. It utilizes an AVL FTIR i60 spectrometer with the high spectral resolution of 0.5 cm-1 for fast transient gas phase analysis. The FTIR uses a silicon nitride (Si3N4) IR and a photoconductive MCT (HgCdTe) detector. The sample gas cell is an optimized, multi-reflection design with an optical path length of 3.2 m. The system is optimized to generate good detection limits with a system response time of 2 s for the time synchronized measurement of CVS diluted automotive exhaust. The limits of detection for NO and NO2, the two main components of NO_X emissions, were 10000 ppm and 1000 ppm, respectively.

Engine lubricant and coolant temperatures were kept at 80 ± 3 °C and 88 ± 3 °C, respectively, and were controlled in a closed-loop control system developed in-house using K-type thermocouples and a PI control strategy actuating on two solenoid valves.

The in-cylinder pressure was acquired using an AVL GH14-D piezoelectric transducer and an AVL FlexIFEM piezo 2P2E signal conditioner unit. The converted charge-to-voltage signal was crank angle related via the 1440 pulses per revolution encoder signal. It was used to trigger cycle pressure signal data acquisition while the encoder reference signal was used to position the TDC. A NI USB 6351 data acquisition board was used to acquire the externally clocked variable frequency pressure signal. Data was saved and online monitored using the in-house developed DAQMOT combustion analysis software.

Two MPX5700AP pressure transducers were used in the intake and exhaust manifolds to acquire average cycle port pressure. An Endress+Houser Promass Coriolis effect-based gas flow meter (with a maximum measurement error of ±0.35%) was used to measure the 300 kPa pressurized H_2. The injection pressure was attained using two pressure regulators at the exit of the H_2 bottle. Engine-out emissions were not analyzed in this work.

The low-frequency sensor signals, as well as ECU, generated signals were acquired via a low-speed data acquisition system composed of two NI SCXI-1303 modules for thermocouples, an NI SCXI-1300 module for pressure sensors, an NI SCXI-1325 module for general sensors, and an NI SCXI-1600 communication module. The acquired data was an average of the information received over the last 15 seconds, acquired at a frequency of 1 kHz. Figure 1 presents the engine dynamometer test cell instrumentation scheme.

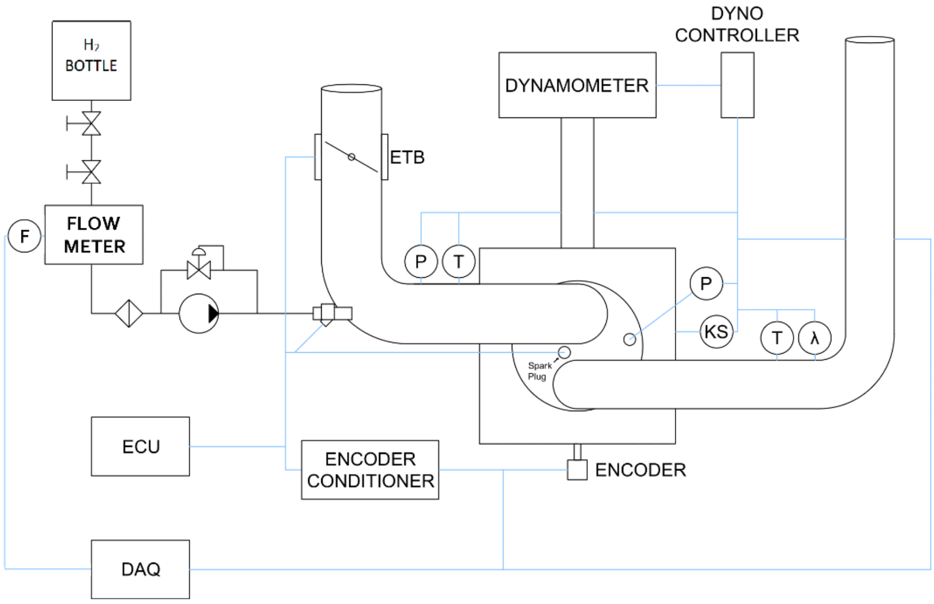

Figure 1 – Engine test cell instrumentation scheme.

The test methodology was based on a fixed throttle position resulting in 98.6 ±0.1 kPa intake pressure. Five load points (2.0, 2.5, 3.5, 4.5 and 5.5 bar IMEP), with near constant excess air ratios (lambda) for each load point were evaluated. A constant injection pulse width was set in the ECU for each load point, and the load slightly varied according to the combustion phasing controlled by the spark. If load deviated more than 3% from the starting point due to better combustion phasing, injection pulse width was modified to keep load constant. Spark sweeps were performed to find the minimal spark advance for the best torque (MBT) starting from the highest air dilution ratio achievable (lowest load) for stable engine operation (COV_{IMEP}) lower than 3.0%. MBT was assigned as the spark advance of the highest indicated mean effective pressure (IMEP) for a constant H_2 injection pulse width. Higher loads were not evaluated as knock tendency increased considerably after 5.5 bar IMEP load, thus, none of the test points evaluated in this work presented knock. IMEP was chosen instead of brake torque due to the nature of the single-cylinder research engine, where brake parameters are not as important as the indicated ones. IMEP and COV_{IMEP} were calculated as

$$IMEP = \frac{\int_{-180}^{540} p_i dV}{V_d} = \frac{W_{c,i}}{V_d} \tag{1}$$

$$COV_{IMEP} = \frac{IMEP_{std}}{IMEP_{average}} \cdot 100 \tag{2}$$

were $p_i, V, V_d, W_{c,i}, IMEP_{std}, and\ IMEP_{average}$ were the instantaneous in-cylinder pressure, instantaneous volume, engine displacement volume, work delivered by the in-cylinder gas during the two-revolution four-stroke cycle, the 100 cycle IMEP standard deviation and its average value, respectively. From the in-cylinder cycle data, combustion heat release rate (HRR) was evaluated using a constant specific heat ratio γ =1.35, and, mass fraction burned (MFB) was evaluated as the integral of the HRR from the spark (SPK) to the end of combustion (EOC) as:

$$HRR = \frac{dQ_{net}}{dCAD} = \frac{\gamma}{\gamma - 1} p_i \frac{dV_i}{dCAD} + \frac{1}{\gamma - 1} V_i \frac{dp_i}{dCAD} \tag{3}$$

$$MFB = \int_{SPK}^{EOC} dQ_{net} \tag{4}$$

$$V_i = V_{TDC} 0.5(CR + 1)\left[\frac{2L}{S} + 1 - \cos\cos(CAD) - \left(\left(\frac{2L}{S}\right)^2 - (CAD)\right)^{\frac{1}{2}}\right] \quad (5)$$

where L and S were the connecting rod length and stroke length, respectively.

From the MFB curve, it was possible to calculate several combustion-related parameters such as CA10, CA50, and CA90 which stands for the end of the flame development phase (CA10), center of combustion (CA50), and end of flame propagation combustion phase (CA90). From this, flame development angle (FDA) was defined as the period between spark and CA10, while flame propagation main phase was defined as the period between CA10 and CA90. These duration parameters were evaluated in the crank angle degrees (CAD) domain, as conventionally presented in the internal combustion engines community worldwide.

Finally, indicated efficiency was used to access engine performance to transform fuel energy into gas work (not considering engine mechanical components friction). It was calculated as:

$$\eta_I = \frac{IMEP.V_d}{m_{H2,c}.LHV_{H2}} \quad (6)$$

where $m_{H2,c}$ was the mass of H_2 injected in the cylinder per cycle (calculated from H_2 flow measurement and engine speed), and LHV_{H2} was the lower heating value of hydrogen of 119.70 $MJ.kg^{-1}$ (Heywood, 2018).

3. RESULTS

It is worth starting by emphasizing that stable engine operation was achieved for excess air ratios up to 4.5. Figure 2 presents the IMEP, PMEP, COV_{IMEP}, NO_X emissions, CA50 (center of combustion), maximum pressure and the angle it occurred (CA Pmax), and exhaust gas temperature of the five tested loads for the different spark timings. As throttle position was kept constant for all loads investigated, Figure 2 (a) shows that variations on IMEP were attributed to the combustion phasing caused by spark timing variation and in a smaller fraction to the variation on intake pressure. Small variations in intake pressure were attributed to the increase in H_2 partial pressure when increasing injection quantity. As expected, the increase in H_2 injection quantity for a fixed intake pressure resulted in the increase in engine load, as more fuel energy was released and transformed into gaseous work each cycle. Adversely, in a conventional SI engine operating at a stoichiometric air-fuel ratio (required for the efficient conversion of CO, unburned hydrocarbons, and NO_X in the three-way catalyst), the load would be controlled by a combination of cam phasing and throttle position. A possible consequence of the lean H_2 operation would be the requirement of a lean NO_X trap or selective reduction catalyst system to manage NO_X emissions under lean conditions. On the other hand, at such lean conditions of the tests, raw NO_X emissions were near zero for loads up to 4.5 bar IMEP at a $\lambda \cong 2.6$.

Lower loads were not tested because the load of 2.0 bar IMEP was slightly higher than that consumed by friction to enable operation at 1800 rpm. Even then, COV_{IMEP} values for lambda around 4.5, as shown in Figure 2 (c), was low enough to imply that higher enleanment would be tolerable under the COV_{IMEP} limit of 3.0%. Higher loads were limited by knock and were not tested in this evaluation. It's worth mentioning that when compared to ethanol, for example, H_2 lean limit was near 4.5 (for this test point), while the ethanol and gasoline lean limit at low loads is in the order of lambda 1.6 and 1.5 for the homogenous operation. These diesel-like air-to-fuel ratios were achievable due to the broad flammability limits of H_2. As presented in the figure, MBT spark timing (marked as a square) was chosen as the highest load and efficiency for the constant intake pressure and lambda. As expected, the spark timing advance reduced the COV_{IMEP} until a point where combustion happened too early in the cycle, from where COV_{IMEP} would increase as a consequence of the low thermal state during the early flame development phase.

According to Figure 2 (e), combustion phasing was totally controlled by the spark timing, and knock occurrence wasn't detected for the presented loads. As also presented in Figure 2 (e), for all tested loads, the increase on spark advance resulted in the advance of the CA50. This is expected as the higher fraction of fuel was burnt during the compression stroke resulting in higher energy being released until the piston reaches TDC. For the MBT operating points, a clear CA50 zone around 10 and 12 CAD ATDC was found while the angle of maximum pressure was delayed from the TDC when decreasing the excess air ratio (increasing the load). In general, CA Pmax, shown in Figure 2 (f), also tended to be delayed from TDC as spark timing was retarded. In Figure 2 (g), the increase in spark advance resulted in lower exhaust gas temperature as consequence of the earlier combustion termination. As a higher fraction of fuel energy was released during combustion period before TDC, maximum in-cylinder pressure tended to be higher for higher spark advances, as can be seen in Figure 2 (h).

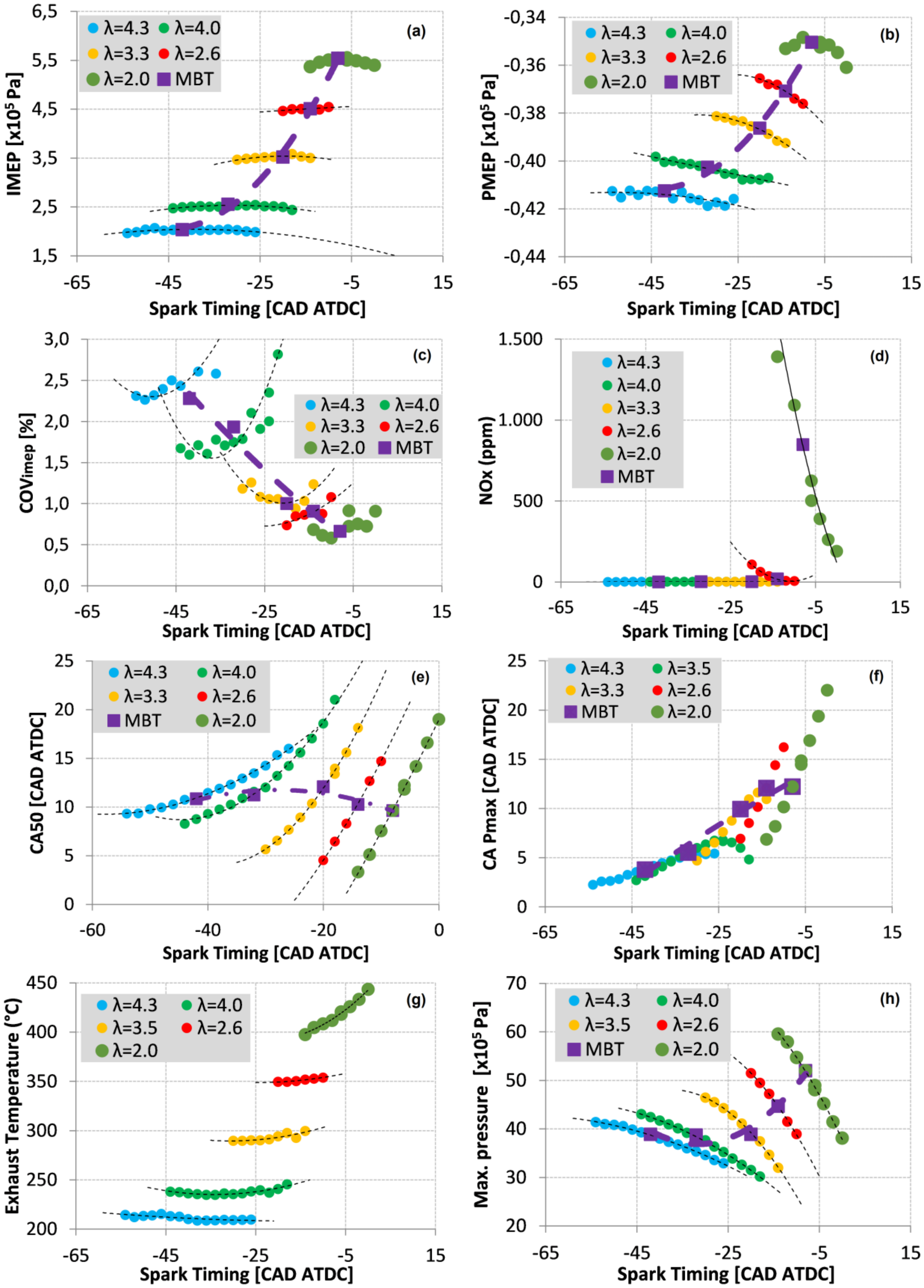

Figure 2 – (a) IMEP, (b) PMEP, (c) COV_{IMEP}, (d) NO_X raw emissions, (e) angle of 50% mass fraction burned (CA50) and (f) angle of maximum pressure, (g) exhaust gas temperature and (h) maximum in-cylinder pressure as a function of spark timing for several air-to-fuel ratios at 1800 rpm and 95.8 kPa intake pressure for several air-to-fuel ratios.

Flame development angle (CA0-10) and flame propagation main phase (CA10-90) durations are presented in Figure 3 (a) and (b), respectively. The increase in CA0-10 with the spark advance for the highest dilution case can be explained by the low in-cylinder pressure and temperature when the spark occurs, which reduced chemical kinetic mechanisms rates. The higher the engine load, the higher the in-cylinder thermal state during the flame kernel growth period and shorter the CA0-10 period. For the less diluted operation cases, the combustion initiation was accelerated with the delay in spark timing, probably as an interaction of initial flame kernel with piston crown which incurred in higher flame front heat transfer. It is worth mentioning that CA0-10 of the MBT cases presented a linear decreasing trend with the increase in engine load (with mixture enrichment) and the same trend was found for CA10-90 of the MBT cases. The near stoichiometric operation at higher loads and higher combustion temperatures increased laminar burning velocities, thus, reducing combustion durations. The same trend can be seen for intermediate excess air ratios (λ =4.0 and 3.5), where after a spark advance point near 25 CAD BTDC, flame development angle tended to increase. This could be caused by a combination of the in-cylinder thermal state and the flame spatial positioning during TDC due to the bowl-in-piston combustion chamber shape. The result of this was that the fastest main phase combustion occurred for CA50 near 12 CAD ATDC, as presented in Figure 6. No trend between CA50 and CA0-10 was found.

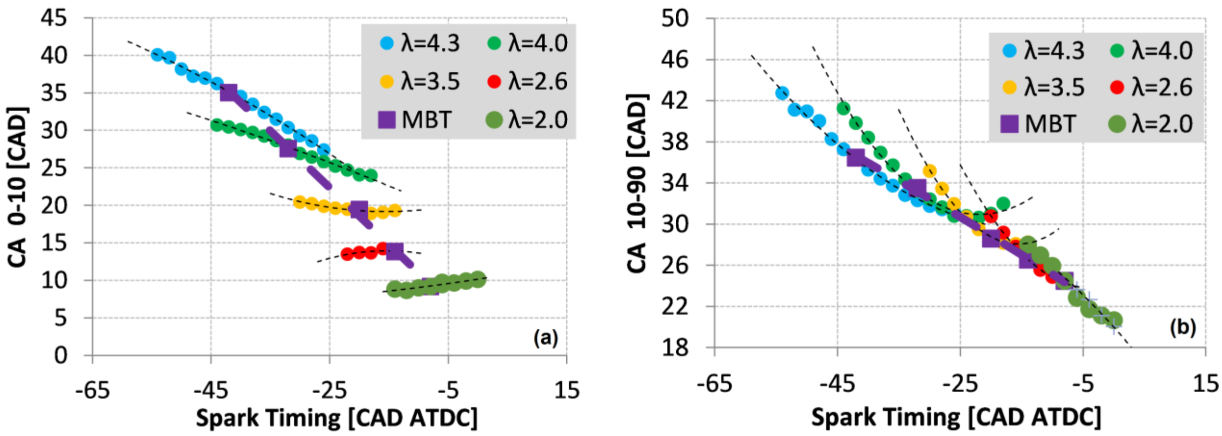

Figure 3 – (a) Flame development angle (CA0-10) and (b) flame propagation main phase duration (CA10-90) at 1800 rpm and 95.8 kPa intake pressure for several air-to-fuel ratios.

Figure 4 (a) presents the indicated efficiency of each excess air ratio for each spark advance tested. As mentioned, the MBT spark advance was set according to the maximum indicated efficiency for each excess air ratio. The reduction in indicated efficiency with the mixture enleanment was mainly a consequence of the longer combustion durations. Ideally, the desired Otto cycle combustion for maximum efficiency would be at constant volume. As real combustion is not instantaneous, a fraction of the heat release must occur before TDC, increasing compression work for the sake of higher expansion work. Longer combustion durations reduced the constant-volume combustion fraction (when pistons were around TDC) and decreased the conversion of fuel energy to piston work efficiency. MBT spark advance points provided the best fuel heat release distribution around TDC. When comparing these indicated efficiency values to the same engine operating with ethanol, Brazilian gasohol and CNG with stoichiometric combustion (for the sake of three-way catalyst reduction of NO_X) at the same engine speed, H_2 lean operation provided higher naturally aspirated efficiencies at the tested load conditions, as presented in Figure 4 (b).

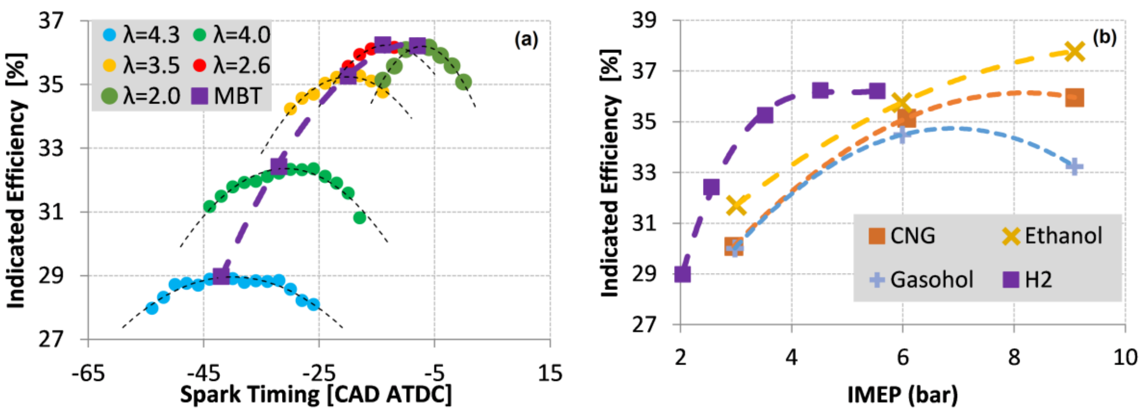

Figure 4 – (a) Effect of spark timing on indicated efficiency at 1800 rpm and 95.8 kPa intake pressure for several air-to-fuel ratios with H_2 and (b) indicated efficiency comparison with ethanol, Brazilian gasohol and CNG at 1800 rpm.

4. CONCLUSIONS

The use of hydrogen as a spark-ignition engine fuel was investigated for several lean excess air ratios. For this, spark sweeps were developed to find the MBT spark advance for each excess air ratio, pointing to:

- Stable engine operation was achieved for lean excess air ratio up to 5.5;
- H_2 faster main phase combustion was found for fixed CA50 around 12 CAD ATDC, while highest efficiency (MBT) CA50 tended to be closer to TDC – the leaner the mixture got, closer to the TDC the CA50 was;
- H_2 operation achieved high indicated efficiency values for the tested loads when compared to ethanol and gasoline operation in a modern direct-injection engine equipped with direct fuel injection;

In this sense, the use of H_2 as an internal combustion fuel not only provided high-efficiency engine operation for the tested engine loads but also assured it as an alternative to decarbonize the transportation sector and decrease its impact on greenhouse gas emissions.

5. ACKNOWLEDGEMENTS

The authors gratefully acknowledge the financial support of Rota Program 2030 - Segment V - FUNDEP (project number: 27192.01.03/2021.02-00). The authors also thank CNPq, CAPES and FAPERGS for the financial support for the laboratory activities and TCA/Horiba Sistemas de Testes Automotivos and Marelli Sistemas Automotivos for supporting the project.

6. REFERENCES

Al-Buraiki, A. S. and Al-Sharafi, A., 2022. "Hydrogen production via using excess electric energy of an off-grid hybrid solar/wind system based on a novel performance indicator." Energy Conversion and Management, Vol. 254, pp. 115270.

Aleiferis, P., Taylor, A., Ishii, K., & Urata, Y. (2004). The nature of early flame development in a lean-burn stratified-charge spark-ignition engine. *Combustion and Flame*, *136*(3), 283–302. https://doi.org/10.1016/j.combustflame.2003.08.011

Heywood, J. B. (2018). *Internal Combustion Engines Fundementals* (2nd ed). McGraw-Hill.

César, A. S.; Veras, T. S.; Mozer, T. S.; dos Santos, D. C. R M.; Conejero, M. A., 2019. "Hydrogen productive chain in Brazil: An analysis of the competitiveness' drivers". Journal of Cleaner Production, Vol. 207, pp. 751 - 763.

IEA, 2019. "The future of hydrogen." <https://iea.blob.core.windows.net/assets/9e3a3493-b9a6-4b7d-b499-7ca48e357561/The_Future_of_Hydrogen.pdf >.

IPCC, 2021. "Sixth Assessment Report." <http://www.ipcc.ch/report/ar6/wg1/downloads/report/IPCC_AR6_WGI_Full_Report.pdf>.

Krishnan Unni, J., Bhatia, D., Dutta, V., Das, L. M., Jilakara, S., & Subash, G. P. (2017). Development of Hydrogen Fuelled Low NOx Engine with Exhaust Gas Recirculation and Exhaust after Treatment. *SAE International Journal of Engines*, *10*(1). https://doi.org/10.4271/2017-26-0074

Lanzanova, T. D. M., Dalla Nora, M., & Zhao, H. (2016). Performance and economic analysis of a direct injection spark ignition engine fueled with wet ethanol. *Applied Energy*, *169*, 230–239. https://doi.org/10.1016/j.apenergy.2016.02.016

Lee, J., Park, C., Bae, J., Kim, Y., Choi, Y., & Lim, B. (2019). Effect of different excess air ratio values and spark advance timing on combustion and emission characteristics of hydrogen-fueled spark ignition engine. *International Journal of Hydrogen Energy*, *44*(45). https://doi.org/10.1016/j.ijhydene.2019.07.181

Minutillo, M.; Perna, Alessandra; Sorce, A., 2020. "Green hydrogen production plants via biogas steam and autothermal reforming processes: energy and exergy analyses". Applied Energy, Vol. 277, pp. 115452.

MME, 2021. "Programa Nacional do Hidrogênio (PNH2)." <http://www.gov.br/mme/pt-br/assuntos/noticias/mme-apresenta-ao-cnpe-proposta-de-diretrizes-para-o-programa-nacional-do-hidrogenio-pnh2/HidrognioRelatriodiretrizes.pdf >.

Reuters, 2022. "Commodities News, Commodity Trading Prices & Data." < http://www.reuters.com/finance/commodities/beta>.

Tang, X., Kabat, D. M., Natkin, R. J., Stockhausen, W. F., & Heffel, J. (2002). Ford P2000 hydrogen engine dynamometer development. *SAE Technical Papers*. https://doi.org/10.4271/2002-01-0242

Verhelst, S., Sierens, R., & Verstraeten, S. (2006). A critical review of experimental research on hydrogen fueled SI engines. *SAE Technical Papers*. https://doi.org/10.4271/2006-01-0430

Younas, M.; Shafique, S.; Hafeez, A.; Javed, Fahad; Rehman, F., 2022. "An overview of hydrogen production: current status, potential, and challenges." Fuel, Vol. 316, pp. 123317.

7. RESPONSIBILITY NOTICE

The author(s) is (are) the only responsible for the printed material included in this paper.